Climate Dynamics (2026) 64:38
https://doi.org/10.1007/s00382-025-08019-6

ORIGINAL ARTICLE

An observational study of the modulation of the diurnal variations by the intraseasonal oscillations of the Indian summer monsoon

Vasubandhu Misra[1,2] · **C. B. Jayasankar**[2]

Received: 1 July 2025 / Accepted: 7 December 2025

Abstract

We show strong diurnal variations of precipitation over parts of the tropical Indian Ocean including the northern Bay of Bengal, eastern Arabian Sea (off the west coast of India) and in the equatorial Indian Ocean, and over eastern Himalayan foothills using NASA's Integrated Multi-Satellite Retrievals for Global Precipitation Mission version 7 (IMERG) rainfall analysis. The amplitudes of these diurnal variations of precipitation over these oceanic regions of the tropical Indian Ocean in the May through September (MJJAS) period exceed that over the neighboring land. Our analysis suggests that these diurnal variations over the oceans (northern Bay of Bengal and southeastern Indian Ocean off the coast of Sumatra) are strongly modulated by the passage of both the high-frequency (10–20 days) and the low-frequency (20–70 days) Intra-Seasonal Oscillations (ISOs) in the MJJAS period. The diurnal amplitudes over these oceanic regions amplify or dampen during the wet or dry spells of both the high and low frequency ISOs, respectively. We also find that both the ISOs have comparable influence on the diurnal variations. However, the coincidence of the wet spells of both the ISOs further amplifies the diurnal amplitude of the rainfall over northern Bay of Bengal.

1 Introduction

Diurnal variability of precipitation is one of the fundamental modes of climate variability, especially in the tropics (Yang and Slingo 2001). They indicate that validating a climate model simulation to diurnal variability is a key test of its fidelity given that diurnal variability is one of the basic, forced modes of the climate system, which manifests from the complex interactions between the land–atmosphere-ocean-cryosphere system. The verification of the diurnal cycles of precipitation is also often used to test the efficacy of the model physical parameterization schemes (e.g., Dai et al. 1999; Dirmeyer et al. 2012; Niu et al. 2020). The diurnal cycle of rainfall in the Indian Summer Monsoon (ISM) plays a critical role in modulating the surface hydrology, convective processes, and even the large-scale divergent circulations (e.g., Kishtawal and Krishnamurti 2001; Basu 2007; Kumar et al. 2008). The ISM is characterized by a variety of rain features like the ITCZ, low pressure systems, orographic forced rain on the windward slopes, organized mesoscale convective systems, cyclones, and trailing ends of extra-tropical systems (Rao 1976; Das 1986; Basu 2007). But critical to all these features is the near omnipresence of the diurnal variations from mesoscale circulations such as land-sea breezes, katabatic-anabatic winds, mountain valley winds, besides the modulation of surface heat fluxes from ground heating through solar insolation and atmospheric tides (Woolnough et al. 2004; Basu 2007).

The study of diurnal variations of precipitation of ISM has evolved over the years. The scarcity of high temporal resolution observations to resolve this sub-daily variation of precipitation has been a challenge across the tropics, which is now slowly being overcome by new satellite retrieved products. For instance, earlier studies were confined to limited regions that had these high-resolution observations and many of them primarily used surface observations (e.g., Gray and Jacobson 1977; McGarry and Reed 1978; Albright et al. 1981; Prasad 1970, 1974; Haldar et al. 1991; Puri et al. 1994). These studies evolved gradually to using satellite derived cloudiness, brightness temperatures, and precipitation that had larger spatial coverage than some of the earlier studies (e. g., Albright et al. 1985, Hendon and Woodberry

✉ Vasubandhu Misra
vmisra@fsu.edu

[1] Department of Earth, Ocean and Atmospheric Science, Florida State University, Tallahassee, FL, USA

[2] Center for Ocean-Atmospheric Prediction Studies, Florida State University, Tallahassee, FL, USA

Published online: 06 January 2026

1993, Garreaud and Wallace 1997, Ohsawa et al. 2001, Yang and Slingo 2001, Nesbitt and Zipser 2003, Tan et al. 2019a, b, c, 2021). Many of these studies showed that convective precipitation in the tropics generally tended to occur early in the morning over the open oceans and in late afternoon/early evening over land. However, there are many exceptions to this with some studies noting an afternoon maximum in cloudiness and precipitation over some regions of the tropical oceans (e. g., Shin et al. 1990; Yang and Slingo 2001; Serra and McPhaden 2004) and early morning maximum over some terrestrial regions (e.g., Negri et al. 2002; Bhatt and Nakamura 2005; Yang and Smith 2006; Kikuchi and Wang 2008). Furthermore, Yu et al. (2022) identified that the early morning precipitation peak is primarily attributed to long-duration rainfall events exceeding six hours, while the late afternoon peak is predominantly associated with shorter rainfall events lasting less than three hours.

With the advent of the Integrated Multi-satellite Retrievals for Global Precipitation Mission (GPM; Huffman et al. 2020), high-resolution precipitation data has become available at sub-daily scales globally. These datasets offer better spatial detail and improved detection of rainfall features (Tan et al. 2019a, b, c). Tan et al. (2019a, b, c) validated this remotely sensed precipitation product with ground-based observations and showed a reasonable fidelity with the diurnal cycle exhibiting a slight lag of no more than an hour. Furthermore, using this GPM dataset Tan et al. (2021) highlights regional variabilities in phase and amplitude of the diurnal cycle of precipitation, with a focus on the Maritime Continent and South Asia.

Several studies have examined the interactions of the diurnal variations with other temporal scales. For example, Singh and Nakamura (2010) using Tropical Rainfall Measuring Mission (TRMM) data over a period of 10 years found that the foothills of Himalayas had stronger diurnal variability of rainfall during the intraseasonal wet spells of the ISM. In contrast, over central India they find that the diurnal convective rainfall is stronger during dry intraseasonal spells of the ISM. On the other hand, Deshpande and Goswami (2014) using hourly rainfall data over 91 stations across India over a 36-year period find that over central India the diurnal anomalies of precipitation are stronger in active spells compared to break phases of the intraseasonal oscillations of the ISM. They also indicate regional variations in the diurnal cycle of rainfall amongst the coastal, interior, and near orographic regions of India, which point to the different associated circulation and thermodynamic variations. For example, Deshpande and Goswami (2014) find that the diurnal anomalies of rainfall are small in both active and break phases of the ISM along the west coast.

In this study, we utilize the latest version 7 of 27 years (1998–2024) gridded rainfall analysis from GPM at half hourly interval (Huffman et al. 2023, 2024) to analyze the variations of the diurnal variability of the ISM associated with the Intra-Seasonal Oscillation (ISO) of the ISM. This dataset covers both the terrestrial and oceanic regions. Furthermore, since this dataset is available globally, we are able to use a spatially larger domain to analyze the variations of the diurnal variability of ISM that covers southeast Asia as well.

We identify two distinct scales of ISO that correspond to 10–20 days, referred as High-Frequency (HF) ISO (Krishnamurti and Bhalme 1976; Krishnamurthy and Shukla 2007; Karmakar et al. 2017) and 20–70 days or Low-Frequency (LF) ISO (Sikka and Gadgil 1980; Yasunari 1980). Besides their distinct temporal scales, HFISO propagates in the northward and eastward direction whereas LFISO is characterized by northward and westward propagation of convection (Krishnamurthy and Shukla 2007; Karmakar and Misra 2020). To our knowledge, this is the first time we will be examining the interactions of the diurnal variations of precipitation with these two distinct scales of ISOs of the ISM. In the following section we provide a description of the data, and the diagnostic methods used in the analysis. This is followed by the description of results in Sect. 3 with concluding remarks in Sect. 4.

2 Data and diagnostic methods

In this study we use NASA's Integrated Multi-Satellite Retrievals for Global Precipitation Mission version 7 (IMERG) gridded rainfall analysis (Huffman et al. 2023, 2024). This data is at 0.1° grid resolution, at 30 min temporal resolution from 1998 to the present (26 years). This is an unprecedented dataset in terms of its spatio-temporal resolution with global coverage for over 25 years, which allows for studying diurnal variations and intraseasonal variations of precipitation with adequate sample size for developing robust conclusions. This dataset and its previous versions have been extensively validated with instantaneous passive microwave retrievals and ground measurements and is shown to have reasonable fidelity (Murali Krishna et al. 2017; Tan et al. 2019a; Huffman et al. 2020; Pradhan and Indu 2021; Da Silva et al. 2021; Prakash and Srinivasan 2021; Ageet et al. 2022; Gautam and Pandey 2022; Yu et al. 2022; Gentilucci et al. 2022; Ghimire et al. 2022; Huffman et al. 2023, 2024). It is now widely used for model validation studies (e.g., Christopoulos and Schneider 2021; Tai et al. 2021; Misra and Jayasankar 2025). Daily precipitation from IMERG has also been verified over the tropical oceans using buoy observations and are shown to be in good agreement (Pradhan and Markonis 2023). Furthermore, Pradhan et al. (2022) note that the successive versions of IMERG

have shown substantial improvement over the previous version over all spatio-temporal scales globally, suggesting that it is on a promising path for becoming a reliable validation dataset.

The diurnal variations of this rainfall analysis were also evaluated against ground observations (Tan et al. 2019b; Watters and Battaglia 2019; Anjana and Singh 2024). They showed that IMERG exemplified in its ability to capture diurnal variations of precipitation globally. We also made use of the daily rainfall data from the Asian Precipitation – Highly-Resolved Observational Data Integration Towards Evaluation (APHRODITE; Yatagai et al. 2012) to validate the climatological rainfall from IMERG over the region. APHRODITE analysis is based on a dense network of rain gauge data that is quality controlled. APHRODITE data is available on a 0.25° grid from 1951 to 2015 and nearly coinciding with the domain shown in Fig. 1. Unlike IMERG, APHRODITE is only available at daily interval and over the terrestrial region of the domain. We use the last 26 years from 1992 to 2015 of the APHRODITE data to make the climatology comparable with the corresponding climatology from IMERG.

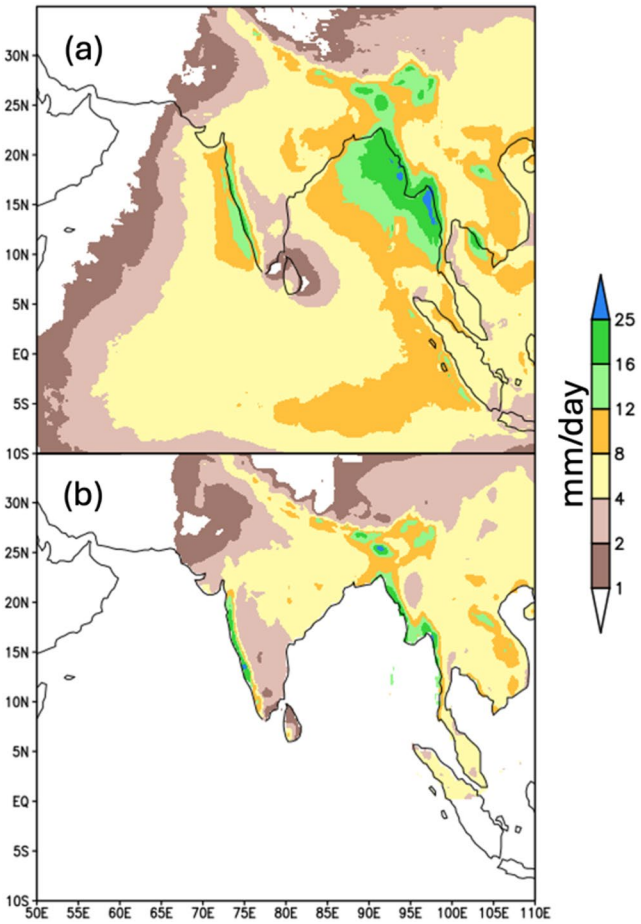

Fig. 1 The climatological (1998–2023) mean of May through September (MJJAS) from **a** IMERG and **b** APHRODITE observations

To filter intraseasonal oscillations and diurnal variations we use the Multi-dimensional Ensemble Empirical Mode Decomposition (MEEMD; Wu et al. 2009; Feng et al. 2014; Misra and Jayasankar 2023). Ensemble Empirical Mode Decomposition (EEMD) is a data adaptive signal processing approach, which decomposes the timeseries into discrete Intrinsic Mode Functions (IMFs) which can be regarded as basis functions that are determined by the timeseries itself (Huang and Wu 2008). The IMFs are obtained via a sifting process that involves identifying local extrema (both maximum and minimum points) and connecting these points with a cubic spline to create upper and lower envelopes. A 'component' is then obtained by calculating the difference between the data and the local mean of the upper and lower envelopes. This two-step procedure is repeated until the two envelopes are symmetric around zero or within a certain tolerance, resulting in the 'component' being identified as the first IMF. The sifting process is considered complete when the residue, which is the difference between the IMFs and the original data, produces a monotonic function containing one internal extremum from which no additional IMFs can be extracted. EEMD is a noise-assisted data analysis, wherein the IMFs are determined by an ensemble of (500) trials generated from adding Gaussian white noise to the timeseries (Wu and Huang 2009). This process avoids mode mixing and automatically projects to the proper scales of reference established by the background white noise. However, applying this EEMD procedure at every grid point of a domain as large as the southeast Asian domain for this study is impractical. Therefore, the MEEMD approach involves using EOF analysis and then conducting EEMD on the first 10 Principal Components (PCs) that explain the most variance. The variable anomaly is then reconstructed back by only retaining the IMFs in each of the PCs and multiplying it with the corresponding EOF (Misra and Jayasankar 2023). The first 10 EOFs retained in the analysis of precipitation is sufficient as the variance explained begins to asymptote after the first 10 PCs.

The amplitude of the diurnal variations is noted from the maximum rainfall of the day from the filtered precipitation anomalies at diurnal scales from MEEMD. Similarly, the phase of the diurnal cycle is obtained by the time of the day of maximum of the filtered precipitation anomalies at the diurnal scales. The phase of the diurnal cycle of precipitation is expressed in Local Solar Time (LST).

3 Results

3.1 Climatology

Figure 1a shows the climatological rainfall from IMERG for the May through September (MJJAS) period and the corresponding climatology from APHRODITE in Fig. 1b. The precipitation maxima along the western Ghats and northeast hills in India, Arakan Yoma and Bilauktaung ranges in Myanmar have similar correspondence in both datasets. Similarly, the precipitation minima over northwest and southeastern peninsular India and Sri Lanka are comparable in the two datasets. There are however some subtle differences between them including the over estimation over eastern China, the northeast hills of India, and the southeastern peninsular India in IMERG relative to APHRODITE. Notwithstanding these differences and acknowledging its extensive validation over the region in other studies (e.g., Tan and Santo 2018; Mitra et al. 2018; Lee et al. 2019; Da Silva et al. 2021; Gautam and Pandey 2022) it can be stated that IMERG provides a reliable high-resolution dataset of precipitation over the southeast Asia.

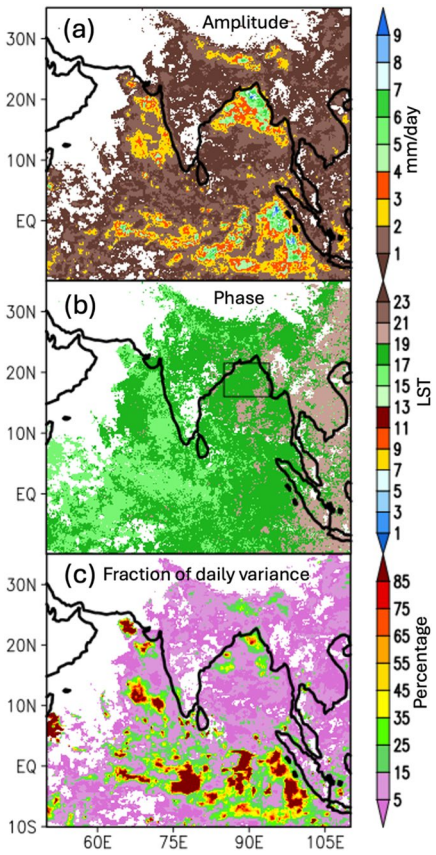

Fig. 2 The climatological mean May–June-July–August-September (MJJAS) diurnal **a** amplitude (mm/day) and **b** phase (LST) of observed precipitation. The unshaded areas indicate regions where the diurnal variability could not be defined. The rectangular box (85°E-94°E and 16°N-21.5°N) inscribed over northern Bay of Bengal in (**b**) is used in area averaging for subsequent figures. **c** The fraction of daily precipitation in MJJAS explained by diurnal variation and is expressed in percentage

In addition to the rainfall maxima over the terrestrial regions in the domain, we also observe a relatively extensive rainfall maxima over the northern and eastern Bay of Bengal (BoB) region and along the western coast of India. However, Shige et al. (2017) suggest that the infrared-based rainfall estimates in IMERG tend to smear and overestimate the rainfall over a broader coastal ocean upstream of the western Ghats and Arakan Yoma ranges of Myanmar from cold brightness temperatures of associated extensive cirrus anvils. Furthermore, Biswas et al. (2025) indicate that IMERG in comparison to the Indian Meteorological Department (IMD) rainfall analysis underestimates the low intensity (<50 mm/day) rainfall and overestimates high intensity (50–200 mm/day) rainfall over northwestern Himalayas for elevation ranges between 1000 and 5000 m. However, Biswas et al. (2025) indicate that IMERG shows good fidelity in identifying rain events over northwestern Himalayas.

We can robustly generate the climatological diurnal amplitude and its phase (Fig. 2a and b) from IMERG given its temporal coverage of half-hourly interval of precipitation over a 26-year period. Figure 2a shows the climatological diurnal amplitude of rainfall from IMERG is prominent (exceeding 2 mm/day) over northern Bay of Bengal, the eastern Arabian Sea off the western coast of India, the eastern equatorial Indian Ocean and the Himalayan ranges. In contrast, most other regions in the domain have diurnal amplitudes $\leq$ 2 mm/day. It is also interesting to note the comparatively weaker diurnal amplitude over central India, and negligible diurnal variations over parts of southeastern peninsular India, and the semi-arid regions of northwestern parts of India and northern China, and over parts of northern Myanmar and northern Thailand. The corresponding diurnal phase of the precipitation shows a dominance of 17–19 LST across the domain except over Vietnam, Cambodia, parts of Laos, Malaysian Peninsula and parts of Indonesia where the diurnal peak occurs between 19 and 21 LST. The fraction of daily precipitation in MJJAS explained by diurnal variation in Fig. 2c indicates that regions with large amplitudes of diurnal variations (Fig. 2a) shows this fraction to be large relative to other regions that are $\leq$ 15%. In some of these oceanic regions, where the diurnal amplitude of precipitation is relatively large, the fraction of daily precipitation explained by the diurnal scales is over 85% (Fig. 2c). We isolate this region of northern BoB (outlined with a box in Fig. 2b) for further analysis to understand the potential modulation of the diurnal scales in this region by the ISO scales. Although, this region of northern BoB is being isolated, the spatially coherent variations of the ISOs on relatively larger scales will also potentially reflect their influence on the

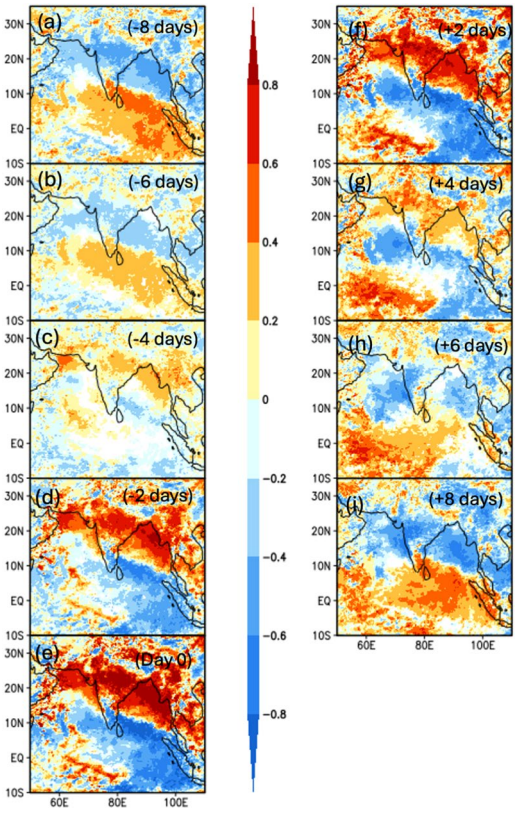

Fig. 3 The regression of the precipitation anomalies of the High-Frequency (10–20 days) Intra-Seasonal Oscillations (HFISO) on the corresponding area averaged HFISO precipitation anomalies over northern Bay of Bengal (BoB; box in Fig. 2b) at different lead/lags at intervals of 2 days over the May through September period of the year. The lead/lag in days is shown in the top right corner of each panel. The – and + values in days suggest that the northern BoB intraseasonal anomalies lag and lead the corresponding intraseasonal anomalies in the rest of the domain, respectively. The shaded regions are statistically significant at 5% significance level according to t-test, values that are not statistically significant are shown in white

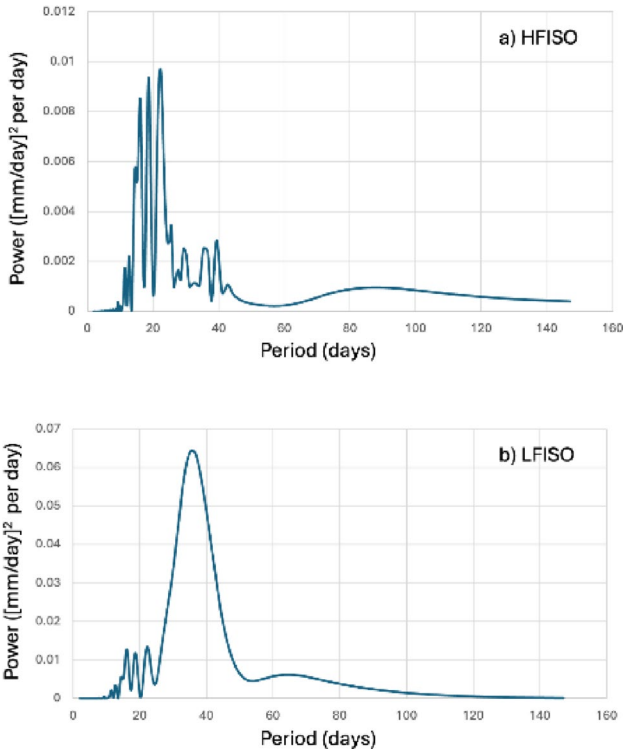

Fig. 4 The power spectrum of the filtered precipitation anomalies for MJJAS season (averaged over 26 years) over the northern BoB region (see box outline in Fig. 2b) for a) HFISO and b) LFISO

diurnal scales of precipitation in other regions of the domain as will be noted in the subsequent sections.

3.2 Intra-seasonal variations

As noted earlier, the ISOs of the ISM have two explicit scales of HF (10–20 days) and LF (20–70 days) variability. The composite structure of the HFISO precipitation anomalies is shown as a regression on the corresponding HFISO anomalies over northern BoB domain (outlined in Fig. 2b) at different lead and lags at intervals of 2 days in Fig. 3. The power spectrum of the filtered HFSIO precipitation anomalies over the northern BoB domain is shown in Fig. 4a, which displays comparatively large power in the 10–20 days band compared to other time scales. It is clearly seen that the positive and negative precipitation anomalies propagate northward from equatorial Indian Ocean towards the foothills of the Himalayas over the course of the 16 days shown in Fig. 3. The amplitude of the HFISO composite precipitation anomalies in Fig. 3 is largest over the northern BoB domain and spans across central India in the west and even further west towards the Arabian Sea with a southeast-northwest tilt as noted in earlier studies (Krishnamurthy and Shukla 2007; Karmakar and Misra 2020).

Similarly, the composite precipitation LFISO anomalies at intervals of 5 days in Fig. 5 show a northward propagation of the anomalies from the equatorial Indian Ocean towards northern India with a similar tilt of southeast-northwest orientation. Once again central India and the neighboring oceans display the largest anomalies of the LFISO as noted in other studies (Krishnamurthy and Shukla 2007; Kulkarni et al. 2011). The power spectrum of the LFISO precipitation anomalies isolated by multi-dimensional EEMD show a spectral peak of around 35 days over the northern BoB in Fig. 4b. Furthermore, the spectral power in LFISO over northern BoB in Fig. 4b is higher than the corresponding HFISO precipitation anomalies in Fig. 4a. It may be noted in Fig. 4b, that LFISO filtered anomalies also contain some power in the HFISO scales, which is an artifact of their weak signals leaking through the various IMFs from the EEMD procedure applied on multiple PCs of the EOFs in the MEEMD technique. Nonetheless, there is a clear distinction in the power spectrums of the two ISOs in Fig. 4.

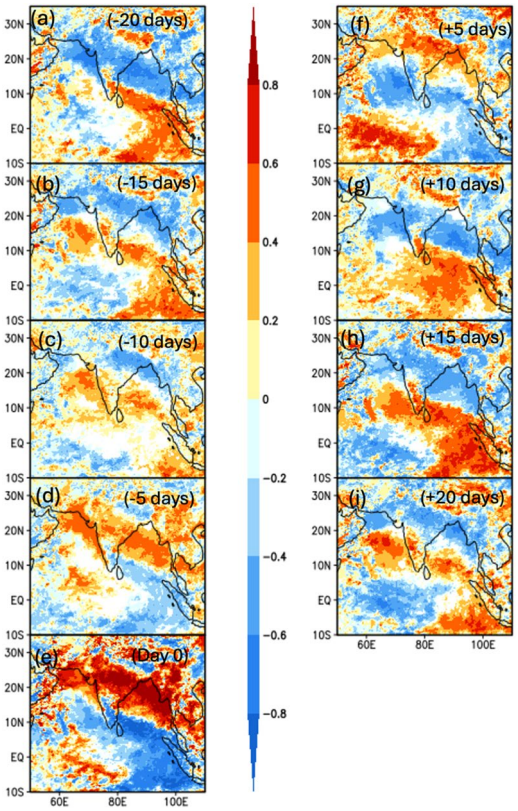

Fig. 5 The regression of the precipitation anomalies of the Low-Frequency (20–40 days) Intra-Seasonal Oscillations (LFISO) on the corresponding area averaged LFISO precipitation anomalies over northern Bay of Bengal (BoB; box in Fig. 2b) at different lead/lags at intervals of 5 days over the May through September period of the year. The lead/lag in days is shown in the top right corner of each panel. The – and + values in days suggest that the northern BoB intraseasonal anomalies lag and lead the corresponding intraseasonal anomalies in the rest of the domain, respectively. The shaded regions are statistically significant at 5% significance level according to t-test, values that are not statistically significant are shown in white.

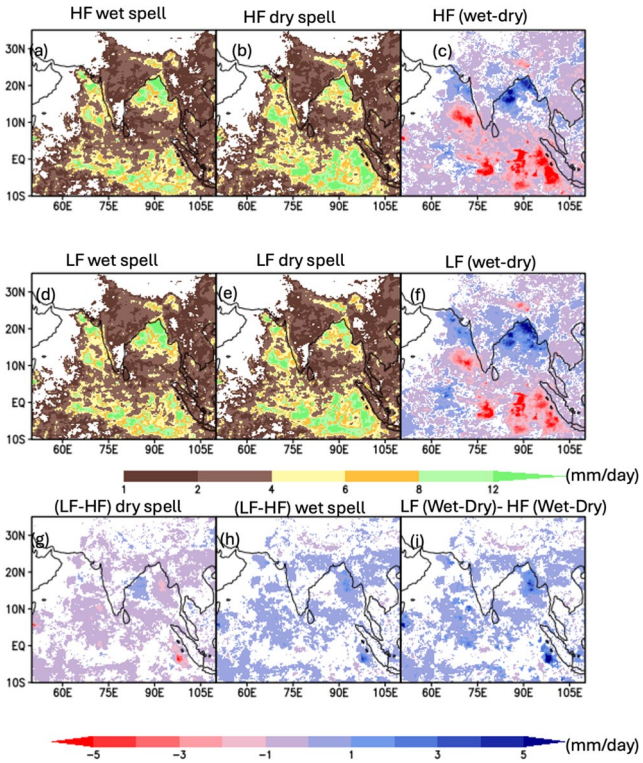

Fig. 6 The composite diurnal amplitude of precipitation based on **a**, **d** wet **b**, **e** dry spells of **a**, **b** High-Frequency (HF) and **d**, **e** Low-Frequency (LF) intraseasonal oscillations over northern Bay of Bengal (box outlined in Fig. 2b). The composite difference between the LF and HF ISOs for **g** dry and **h** wet spells and (**i**) (**c**–**f**). The units in all panels are in mm/day. Only significant values at 5% significance level according to t-test are shaded for the differences

3.3 The modulation of the diurnal amplitude by the intraseasonal variations

We composited the diurnal amplitude of the precipitation anomalies for wet and dry spells of HFISO over northern BoB and find that the largest differences reside over northern BoB, equatorial Indian Ocean, and parts of Arabian coast of India (Fig. 6a–c). Likewise, the largest differences appear over northern BoB, northeastern Arabian Sea, and equatorial Indian Ocean for composites of diurnal precipitation anomalies for wet and dry spells of LFISO (Fig. 6d–f). Here, although the composites have been created with respect to the wet and dry spells of the ISOs over the northern BoB domain, its influence on the diurnal scales in other regions of the domain is apparent because of the spatially coherent structures of the former. For instance, the composite differences in Fig. 6 show an enhancement of the diurnal amplitude of precipitation over northern BoB during the corresponding wet spells of the ISOs with simultaneous diminution of the diurnal amplitude of precipitation over the equatorial Indian Ocean and southeastern Arabian Sea where dry spells of the ISOs are occurring. This is consistent with the banded structures of the ISO precipitation anomalies seen earlier in Figs. 3 and 5. The differences in Fig. 6g–i, suggest that the contrast in the diurnal amplitude of precipitation over many parts of the domain including BoB, Arabian Sea, equatorial Indian Ocean, and over some of the other terrestrial regions in the domain is comparable between LFISO and HFISO.

To understand the diurnal modulation by the ISOs further, we composited the diurnal anomalies during wet spells of HFISO that coincide with the wet spells of LFISO (Fig. 7a) and separately with dry spells of LFISO (Fig. 7b) and find that the differences between these composites (Fig. 7c) reveal the contrast in the modulation of the diurnal variations of precipitation between the two ISOs. Figure 7c indicates that when the wet spells of the HFISO and LFISO coincide, then the diurnal anomalies of precipitation are the largest, i.e., diurnal scales of precipitation amplify the most

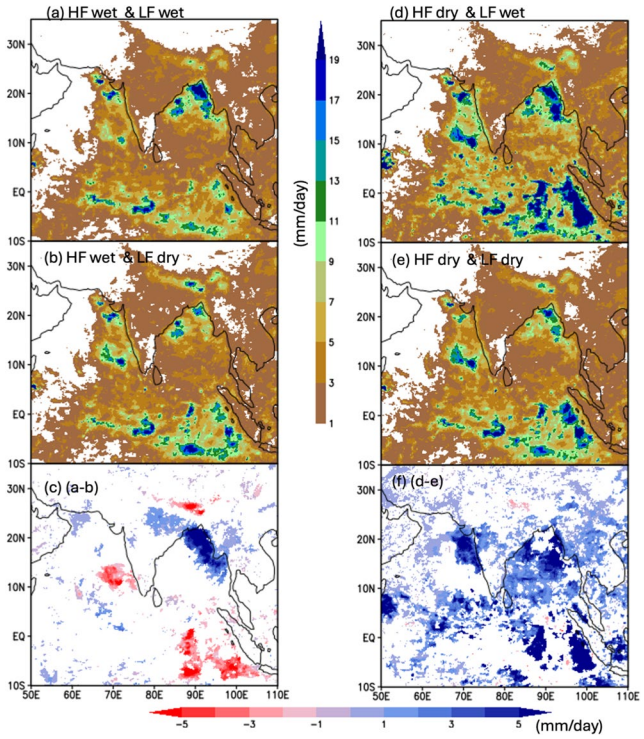

Fig. 7 The composite of the diurnal amplitude of precipitation during the wet spells of High Frequency (HF) Intra-Seasonal Oscillation (ISO) coinciding with **a** wet spells of Low Frequency (LF) and **b** dry spells of LFISO. **c**, **a**, **b**. The composite of the diurnal amplitude of precipitation during the dry spells of HFISO coinciding with **d** wet spells and **e** dry spells of LFISO. **f**, **d**, **e** The units are in mm/day. Only significant values at 5% significance level according to t-test are shaded for the differences

over northern BoB. In contrast, when the HFISO dry spells coincide with the dry spells of the LFISO then the diurnal anomalies of precipitation are comparatively weaker (Figs. 7e and f) relative to dry spell of HFISO coinciding with wet spell of LFISO (Fig. 7d). This also explains the reason for the diurnal composites of rainfall during HFISO being comparatively weaker than LFISO (Fig. 6i) since the likelihood of the wet spells of HFISO coinciding with the dry spells of LFISO are equally likely as coinciding with the wet spells of LFISO owing to the higher frequency of HFISO. Similar differences in the modulation of the diurnal scales of precipitation by HFISO and LFISO is also observed over the eastern equatorial Indian Ocean and the Arabian Sea.

4 Conclusions

This study examines the variations diurnal variations of the Indian Summer Monsoon (ISM) rainfall in the context of its modulation by the Intra-Seasonal Oscillations (ISOs). The ISOs of the ISM have two distinct bands of variability, one in the 10–20 days range which is referred as the High Frequency (HF) ISO and the other in the 20–70 days range which is the Low Frequency (LF) ISO. The study is conducted with 26 years (1998–2023) of NASA's Integrated Multi-Satellite Retrievals for Global Precipitation Mission version 7 (IMERG) gridded rainfall analysis, available on $0.1° \times 0.1°$ grid spacing at half-hourly interval. The IMERG rainfall analysis shows a reasonable verification of the ISM rainfall with APHRODITE data, which is based on rain gauge measurements. The diagnosed diurnal variations of ISM precipitation for the months of May through September indicate that some of the oceanic regions like the northern Bay of Bengal (BoB), equatorial Indian Ocean, and eastern Arabian Sea along the west coast of India besides the foothills of the Himalayas display a stronger diurnal variation compared to neighboring terrestrial regions. The peak of the diurnal variations of precipitation in these regions are between 17 and 19 LST and appear to be spatially homogeneous with parts of southeast Asia (e.g., Vietnam, Cambodia, peninsular Malaysia, parts of Laos and Indonesia) showing a diurnal peak between 19 and 21 LST. IMERG also displays a robust HFISO and LFISO, across the domain with its anomalies propagating from south to north from the equatorial Indian Ocean towards the foothills of the Himalayas with a southeast-northwest tilt of coherent precipitation bands.

Our analysis reveals that wet or dry spells of both ISOs are associated with stronger or weaker diurnal anomalies of precipitation, respectively. The composite anomalies of diurnal precipitation during wet and dry spells of the ISOs over northern BoB confirm these relationships in addition to suggesting that LFISO modulates the diurnal variations more strongly than HFISO. Although, the composites are based on the wet and dry spells of the ISOs over northern BoB, the spatially coherent banded structures on comparatively larger scales of the ISOs force similar modulation of the diurnal scales over other regions in the domain (e.g., equatorial Indian Ocean, southeastern Arabian Sea).

Given the distinct frequencies of the HFISO and LFISOs it is plausible to anticipate constructive or destructive interferences between them. It is shown that constructive or destructive interference of the wet and dry spells of the HFISO with LFISO can further amplify or weaken their influence on the diurnal modulation of the rainfall over northern BoB. Although the focus of this study was over a domain in northern BoB, the large-scale coherent structures of the ISOs also extend simultaneously their influence in other parts of the domain like the equatorial Indian Ocean and southeastern Arabian Sea, where the diurnal variability of precipitation is also significant.

The study has been primarily conducted with rainfall analysis. We will follow this study with a modeling

experiments to further understand the dynamic and thermodynamic aspects of this cross-scale interactions in a future work.

Acknowledgements We acknowledge the support from NASA grant 80NSSC22K0595.

Data availability The half-hourly IMERG v7 rainfall dataset is available from the NASA GES DISC (https://gpm1.gesdisc.eosdis.nasa.gov/data/GPM_L3/GPM_3IMERGHH.07/). The APHRODITE data is publicly available from http://www.chikyu.ac.jp/precip/.

Declarations

Conflict of interest The authors declare that there no potential conflict of interest in this paper.

References

Ageet S, Fink AH, Maranan M, Diem JE, Hartter J, Ssali AL, Ayabagabo P (2022) Validation of satellite rainfall estimates over equatorial East Africa. J Hydrometeorol 23(2):129–151

Albright MD, Mock DR, Recker EE, Reed RJ (1981) A diagnostic study of the diurnal rainfall variation in the GATE. B-Scale Area J Atmos Sci 38:1429–1445

Albright MD, Recker EE, Reed RJ, Dang R (1985) The diurnal variation of deep convection and inferred precipitation in the central tropical Pacific during January–February 1979. Mon Wea Rev 113:1663–1680

Anjana VS, Singh C (2024) Scrutinizing diurnal scale rainfall variability over Himachal Pradesh using high resolution satellite-based GPM IMERG product. J Indian Soc Remote Sens. https://doi.org/10.1007/s12524-024-01923-0

Basu BK (2007) Diurnal variation in precipitation over India during the summer monsoon season: observed and model predicted. Mon Wea Rev 135:2155–2167

Bhatt BC, Nakamura K (2005) Characteristics of monsoon rainfall around the Himalayas revealed by TRMM precipitation radar. Mon Weather Rev 133:149–165. https://doi.org/10.1175/MWR-2846.1

Biswas S, Singh C, Bharti V (2025) An assessment of GPM IMERG version 7 rainfall estimates over the North West Himalayan region. Atmos Res 315:107910. https://doi.org/10.1016/j.atmosres.2025.107910

Christopoulos C, Schneider T (2021) Assessing biases and climate implications of the diurnal precipitation cycle in climate models. Geophys Res Lett 48(13):e2021GL093017

Da Silva NA, Webber BG, Matthews AJ, Feist MM, Stein TH, Holloway CE, Abdullah MF (2021) Validation of GPM IMERG extreme precipitation in the Maritime Continent by station and radar data. Earth Space Sci 8(7):e2021EA001738

Dai A, Giorgi F, Trenberth KE (1999) Observed and model-simulated diurnal cycles of precipitation over the contiguous United States. J Geophys Res Atmos 104(D6):6377–6402

Das PK (1986) Monsoons: Fifth IMO lecture. World meteorological organization, pp. 155.

Deshpande NR, Goswami BN (2014) Modulation of the diurnal cycle of rainfall over India by intraseasonal variations of Indian summer monsoon. Int J Climatol 34(3):793–807

Dirmeyer PA, Cash BA, Kinter JL, Jung T, Marx L, Satoh M, Stan C, Tomita H, Towers P, Wedi N, Achuthavarier D (2012) Simulating the diurnal cycle of rainfall in global climate models: resolution versus parameterization. Clim Dyn 39:399–418

Feng J, Wu Z, Zou X (2014) Sea surface temperature anomalies off Baja California: a possible precursor of ENSO. J Atmos Sci 71:1529–1537

Garreaud RD, Wallace JM (1997) The diurnal march of convective cloudiness over the Americas. Mon Wea Rev 125:3157–3171

Gautam AK, Pandey A (2022) Ground validation of GPM Day-1 IMERG and TMPA Version-7 products over different rainfall regimes in India. Theor Appl Climatol 149(3):931–943

Gentilucci M, Barbieri M, Pambianchi G (2022) Reliability of the IMERG product through reference rain gauges in Central Italy. Atmos Res 278:106340

Ghimire U, Akhtar T, Shrestha NK, Paul PK, Schürz C, Srinivasan R, Daggupati P (2022) A long-term global comparison of IMERG and CFSR with surface precipitation stations. Water Resour Manage 36(14):5695–5709

Gray WM, Jacobson RW (1977) Diurnal variation of deep cumulus convection. Mon Wea Rev 105:1171–1188

Haldar GC, Sud AM, Marathe SD (1991) Diurnal variation of monsoon rainfall in central India. Mausam 42:37–40

Hendon HH, Woodberry K (1993) The diurnal cycle of tropical convection. J Geophys Res 98:16523–16637

Huang NE, Wu Z (2008) A review on Hilbert–Huang transform: the method and its applications on geophysical studies. Rev Geophys 46:RG2006. https://doi.org/10.1029/2007RG000228

Huffman GJ, Bolvin DT, Braithwaite D, Hsu K, Joyce R, Kidd C, Nelkin EJ, Sorooshian S, Stocker EF, Tan J, Wolff DB, Xie P (2020) Integrated Multi-satellitE retrievals for the global precipitation measurement (GPM) mission (IMERG) chapter 19 in Adv. In: Levizzani V, Kidd C, Kirschbaum D, Kummerow C, Nakamura K, Turk FJ (eds) Global change res satellite precipitation measurement, vol 67. Springer Nature, Dordrecht

Huffman GJ, Bolvin R, Joyce EJ, Nelkin J Tan D, Braithwaite, K, Hsu OA, Kelley P, Nguyen S, Sorooshian DC, Watters BJ, West P, Xie (2023) Algorithm theoretical basis document (ATBD) NASA global precipitation measurement (GPM) integrated multi-satellite retrievals for GPM (IMERG) Version 07. PPS, last updated 12 July 2023. 52 pp. https://gpm.nasa.gov/sites/default/files/2023-07/IMERG_V07_ATBD_final_230712.pdf

Huffman GJ, Bolvin DT, Joyce R, Kelley OA, Nelkin EJ, Portier A, Stocker EF, Tan J, Watters DC, West BJ (2024) IMERG V07 release notes. PPS, last updated 26 November 2024, 17 pp. https://gpm.nasa.gov/resources/documents/imerg-v07-release-notes

Karmakar N, Misra V (2020) Differences in northward propagation of convection over the Arabian Sea and Bay of Bengal during boreal summer. J Geophys Res 125:e2019JD031648. https://doi.org/10.1029/2019JD031648

Karmakar N, Chakraborty A, Nanjundiah RS (2017) Space-time evolution of the low- and high-frequency intraseasonal modes of the Indian Summer Monsoon. Mon Weather Rev 145(2):413–435. https://doi.org/10.1175/MWR-D-16-0075.1

Kikuchi K, Wang B (2008) Diurnal precipitation regimes in the global tropics. J Climate 21(11):2680–2696

Kishtawal CM, Krishnamurti TN (2001) Diurnal variation of summer rainfall over the Indian region using 3-hourly gridded rainfall data. J Meteorol Soc Japan 79:259–276

Krishnamurthy V, Shukla J (2007) Intraseasonal and seasonally persisting patterns of Indian monsoon rainfall. J Clim 20(1):3–20. https://doi.org/10.1175/JCLI3981.1

Krishnamurti TN, Bhalme HN (1976) Oscillations of a monsoon system. Part I. Observational aspects. J Atmos Sci 33:1937–1954. https://doi.org/10.1175/1520-0469(1976)033%3c1937:OOAMSP%3e2.0.CO;2

Kulkarni A, Kripalani R, Sabade S, Rajeevan M (2011) Role of intraseasonal oscillations in modulating Indian summer monsoon rainfall. Clim Dyn 36:1005–1021

Kumar S, Rajeevan MN, Sahai AK (2008) Diurnal variations in summer monsoon precipitation in India. Meteorol Atmos Phys 102:105–118. https://doi.org/10.1007/s00703-008-0333-y

Lee J, Lee EH, Seol KH (2019) Validation of Integrated MultisatellitE retrievals for GPM (IMERG) by using gauge-based analysis products of daily precipitation over East Asia. Theor Appl Climatol 137:2497–2512

McGarry MM, Reed RJ (1978) Diurnal variations in convective activity and precipitation during phases II and III of GATE. Mon Wea Rev 106:101–113

Misra V, Jayasankar CB (2023) Characterizing the Madden-Julian Oscillation in the western Pacific Ocean from a regional coupled ocean-atmosphere model simulation. Q J R Meteorol Soc. https://doi.org/10.1002/qj.4620

Misra V, Jayasankar CB (2025) The regional coupled ocean-atmosphere model simulation over eastern tropical Africa. Dyn Atmos Oceans 109:101520. https://doi.org/10.1016/j.dynatmoce.2024.101520

Mitra AK, Kaushik N, Singh AK, Parihar S, Bhan SC (2018) Evaluation of INSAT-3D satellite derived precipitation estimates for heavy rainfall events and its validation with gridded GPM (IMERG) rainfall dataset over the Indian region. Remote Sens Appl: Soc Environ 9:91–99

Murali Krishna UV, Das SK, Deshpande SM, Doiphode SL, Pandithurai G (2017) The assessment of global precipitation measurement estimates over the Indian subcontinent. Earth Space Sci. https://doi.org/10.1002/2017EA000285

Negri AJ, Bell TL, Xu L (2002) Sampling of the diurnal cycle of precipitation using TRMM. J Atmos Ocean Technol 19(9):1333–1344

Nesbitt SW, Zipser EJ (2003) The diurnal cycle of rainfall and convective intensity according to three years of TRMM measurements. J Clim 16:1456–1475

Niu X, Tang J, Wang S, Fu C, Chen D (2020) On the sensitivity of seasonal and diurnal precipitation to cumulus parameterization over CORDEX-EA-II. Clim Dyn 54:373–393

Ohsawa T, Ueda H, Hayashi T, Watanabe A, Matsumoto J (2001) Diurnal variations of convective activity and rainfall in tropical Asia. J Meteorol Soc Japan Ser II 79(1B):333–352

Pradhan A, Indu J (2021) Assessment of SM2RAIN derived and IMERG based precipitation products for hydrological simulation. J Hydrol 603:127191

Pradhan RK, Markonis Y (2023) Performance evaluation of GPM IMERG precipitation products over the tropical ocean buoys. J Hydrometeorol 24:1755–1770

Pradhan RK et al (2022) Review of GPM IMERG performance: a global perspective. Remote Sens Environ 268:11724. https://doi.org/10.1016/j.rse.2021.112754

Prakash S, Srinivasan J (2021) A comprehensive evaluation of near real-time and research products of IMERG precipitation over India for southwest monsoon period. J Remote Sens. https://doi.org/10.3390/rs13183676

Prasad B (1970) Diurnal variation of rainfall in India. Mausam 21:443–450

Prasad B (1974) Diurnal variation of rainfall in Brahmaputra valley. Mausam 25:245–250

Puri SR, Duggal YM, Lal B, Kant R (1994) Some features of hourly rainfall during southwest monsoon season at Delhi. Mausam 45:35–42

Rao YP (1976) Southwest Monsoon. Meteor. Monogr. on synoptic meteorology, No. 1/1976, India meteorological department, 337 pp.

Serra YL, McPhaden MJ (2004) In situ observations of diurnal variability in rainfall over the tropical Pacific and Atlantic Oceans. J Climate 17(18):3496–3509

Shige S, Nakano Y, Yamamoto MK (2017) Role of orography, diurnal cycle, and intraseasonal oscillation in summer monsoon rainfall over the Western Ghats and Myanmar Coast. J Clim 30:9365–9381. https://doi.org/10.1175/JCLI-D-16-0858.1

Shin KS, North GR, Ahn YS, Arkin PA (1990) Time scales and variability of area-average tropical oceanic rainfall. Mon Wea Rev 118:1507–1516

Sikka D, Gadgil S (1980) On the maximum cloud zone and the ITCZ over Indian, longitudes during the southwest monsoon. Mon Weather Rev 108(11):1840–1853. https://doi.org/10.1175/1520-0493(1980)108%3c1840:OTMCZA%3e2.0.CO;2

Singh P, Nakamura K (2010) Diurnal variation in summer monsoon precipitation during active and break periods of central India and southern Himalyan foothills. J Geophys Res. https://doi.org/10.1029/2009JD012794

Tai SL, Feng Z, Ma PL, Schumacher C, Fast JD (2021) Representations of precipitation diurnal cycle in the Amazon as simulated by observationally constrained cloud-system resolving and global climate models. J Adv Model Earth Syst 13(11):e2021MS002586

Tan ML, Santo H (2018) Comparison of GPM IMERG, TMPA 3B42 and PERSIANN-CDR satellite precipitation products over Malaysia. Atmos Res 202:63–76

Tan J, Huffman GJ, Bolvin DT, Nelkin EJ (2019a) Imerg V06: changes to the morphing algorithm. J Atmos Oceanic Technol 36:2471–2482

Tan J, Huffman GJ, Bolvin DT, Nelkin EJ (2019b) Diurnal cycle of IMERG V06 precipitation. Geophys Res Lett 46(22):13584–13592. https://doi.org/10.1029/2019GL085395

Tan J, Hsu KL, Sorooshian S (2019c) The summertime diurnal cycle of precipitation derived from IMERG. J Hydrometeorol 20:947–961. https://doi.org/10.1175/JHM-D-18-0179.1

Tan J, Hsu KL, Sorooshian S (2021) Diurnal cycle of IMERG v06 precipitation. J Hydrometeorol 22:603–620. https://doi.org/10.1175/JHM-D-20-0136.1

Watters D, Battaglia A (2019) The summertime diurnal cycle of precipitation derived from IMERG. Remote Sens 11(15):1781

Woolnough SJ, Slingo JM, Hoskins BJ (2004) The diurnal cycle of convection and atmospheric tides in an aqua planet GCM. J Atmos Sci 61:2559–2573

Wu Z, Huang NE (2009) Ensemble empirical mode decomposition: a noise-assisted data analysis method. Adv Adapt Data Anal 01:1–41. https://doi.org/10.1142/S1793536909000047

Wu Z, Huang NE, Chen X (2009) The multi-dimensional ensemble empirical mode decomposition method. Adv Adapt Data Anal 1:339–372. https://doi.org/10.1142/S1793536909000187

Yang G-Y, Slingo J (2001) The diurnal cycle in the tropics. Mon Weather Rev 129:784–801. https://doi.org/10.1175/1520-0493(2001)129%3c0784:TDCITT%3e2.0.CO;2

Yang S, Smith EA (2006) Mechanisms for diurnal variability of global tropical rainfall observed from TRMM. J Climate 19(20):5190–5226

Yasunari T (1980) A quasi-stationary appearance of 30 to 40 day period in the cloudiness fluctuations during the summer monsoon over India. J Meteorol Soc Jpn 58:225–229

Yatagai A, Kamiguchi K, Arakawa O, Hamada A, Yasutomi N, Kitoh A (2012) APHRODITE: constructing a long-term daily gridded precipitation dataset for Asia based on adense network of rain gauges. Bull Amer Soc 1401–1415. https://doi.org/10.1175/BAMS-D-11-00122.1

Yu L, Leng G, Python A (2022) A comprehensive validation for GPM IMERG precipitation products to detect extremes and drought over mainland China. Weather Clim Extremes 36:100458